Rapid hydrolysis of tertiary isoprene nitrate efficiently removes NO_x from the atmosphere

Krystal T. Vasquez[a], John D. Crounse[b], Benjamin C. Schulze[b], Kelvin H. Bates[a,1], Alexander P. Teng[b,2], Lu Xu[b], Hannah M. Allen[a], and Paul O. Wennberg[b,c,3]

[a]Division of Chemistry and Chemical Engineering, California Institute of Technology, Pasadena, CA 91125; [b]Division of Geological and Planetary Sciences, California Institute of Technology, Pasadena, CA 91125; and [c]Division of Engineering and Applied Sciences, California Institute of Technology, Pasadena, CA 91125

Edited by Mark Thiemens, University of California San Diego, La Jolla, CA, and approved November 3, 2020 (received for review August 17, 2020)

The formation of a suite of isoprene-derived hydroxy nitrate (IHN) isomers during the OH-initiated oxidation of isoprene affects both the concentration and distribution of nitrogen oxide free radicals (NO_x). Experiments performed in an atmospheric simulation chamber suggest that the lifetime of the most abundant isomer, 1,2-IHN, is shortened significantly by a water-mediated process (leading to nitric acid formation), while the lifetime of a similar isomer, 4,3-IHN, is not. Consistent with these chamber studies, NMR kinetic experiments constrain the 1,2-IHN hydrolysis lifetime to less than 10 s in deuterium oxide (D_2O) at 298 K, whereas the 4,3-IHN isomer has been observed to hydrolyze much less efficiently. These laboratory findings are used to interpret observations of the IHN isomer distribution in ambient air. The IHN isomer ratio (1,2-IHN to 4,3-IHN) in a high NO_x environment decreases rapidly in the afternoon, which is not explained using known gas-phase chemistry. When simulated with an observationally constrained model, we find that an additional loss process for the 1,2-IHN isomer with a time constant of about 6 h best explains our atmospheric measurements. Using estimates for 1,2-IHN Henry's law constant and atmospheric liquid water volume, we show that condensed-phase hydrolysis of 1,2-IHN can account for this loss process. Simulations from a global chemistry transport model show that the hydrolysis of 1,2-IHN accounts for a substantial fraction of NO_x lost (and HNO_3 produced), resulting in large impacts on oxidant formation, especially over forested regions.

atmospheric chemistry | isoprene | hydrolysis | organic nitrates | NO_x

The formation of organic nitrates during the oxidation of volatile organic compounds (VOCs) serves to sequester nitrogen oxides (NO_x = NO + NO_2; NO_x, nitrogen oxide free radicals). This chemistry is expected to become increasingly important as NO_x levels decline (1), as has been occurring in the United States (2). Because the formation and subsequent fate of organic nitrates alters the concentrations and distributions of NO_x in the atmosphere, they, by extension, also significantly impact the production of tropospheric ozone and organic aerosols (3–6), which have known impacts on the environment and human health.

Due to the sheer abundance and reactivity of isoprene in the boundary layer, organic nitrates created from its oxidation are believed to greatly affect the atmospheric NO_x lifetime (7–15). Isoprene-derived hydroxy nitrates (IHNs) are formed primarily during the OH oxidation of isoprene in the presence of NO (16) (Scheme 1). Recent laboratory measurements suggest the branching ratio for this pathway (α) is ~13% (17), which is higher than many previous estimates (18). While eight IHN isomers can form (17), two of these isomers (1,2-IHN and 4,3-IHN; Scheme 1) make up the majority of the total IHN yield at atmospherically relevant conditions. Once formed, current understanding suggests that IHNs are primarily lost from the atmosphere through deposition and chemical oxidation (3, 18, 19).

The relative importance of the IHN-loss pathways determines the extent to which NO_x is recycled back into the atmosphere. For instance, deposition results in the permanent removal of NO_x, but the IHN lifetime against deposition under typical atmospheric conditions is relatively long: $\tau_{dep} \approx 24$ h for $v_{dep} = 1.7$ cm s^{-1} (20) and a boundary layer height of 1.5 km. On the other hand, chemical oxidation by OH is more important, providing a lifetime of 9.3 and 6.9 h (assuming [OH] = 1×10^6 molecules cm^{-3}) for 1,2-IHN and 4,3-IHN, respectively (18). Although studies have shown that the nitrate moiety typically remains attached to these molecules following this chemistry (particularly for 4,3-IHN), subsequent photooxidation of second-generation products can still contribute to significant NO_x recycling (21, 22).

Model simulations of field measurements tend to overestimate daytime concentrations of IHN (19, 23–26). While this might be partially due to assumptions made regarding the isomer distribution of isoprene peroxy radicals (RO_2) and α, this discrepancy has also been attributed to a missing IHN sink. Several possible sinks have been hypothesized. It has been suggested that the tertiary nitrate group on 1,2-IHN allows this molecule to hydrolyze rapidly in clouds or in aerosol (24, 27–30). This loss

Significance

Isoprene-derived hydroxy nitrates (IHNs) play a significant role in controlling the lifetime of NO_x. Here, we showcase isomer-specific measurements of IHN in ambient air, which have allowed us to quantify real-time changes in its isomer distribution. These measurements show that 1,2-IHN undergoes a rapid loss not experienced by the 4,3-IHN isomer. Laboratory studies suggest this sink is likely condensed-phase hydrolysis, forming HNO_3. To match observations, one-dimensional box-model simulations require additional loss rates (here, assigned to hydrolysis) similar in magnitude to the accounted loss processes (OH oxidation and dry deposition). Global simulations included in this process show reduced ozone levels and assign a significant fraction of HNO_3 production to this mechanism within the lower atmosphere.

Author contributions: J.D.C. and P.O.W. designed research; K.T.V., J.D.C., B.C.S., K.H.B., A.P.T., L.X., H.M.A., and P.O.W. performed research; J.D.C. and P.O.W. contributed new reagents/analytic tools; K.T.V., J.D.C., and A.P.T. analyzed data; and K.T.V., J.D.C., and P.O.W. wrote the paper.

The authors declare no competing interest.

This article is a PNAS Direct Submission.

[1]Present address: Center for the Environment, Harvard University, Cambridge, MA 02138.

[2]Private address: Daly City, CA 94014.

[3]To whom correspondence may be addressed. Email: wennberg@caltech.edu.

This article contains supporting information online at https://www.pnas.org/lookup/suppl/doi:10.1073/pnas.2017442117/-/DCSupplemental.

First published December 10, 2020.

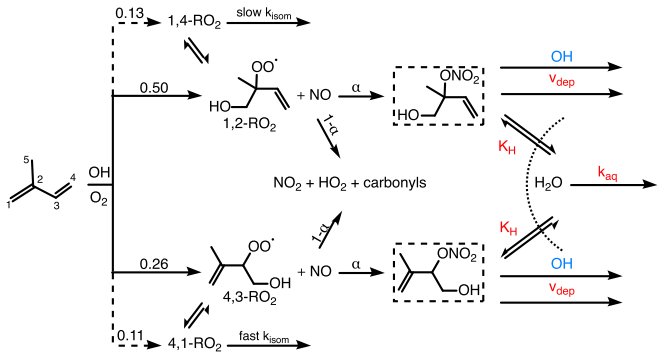

Scheme 1. IHNs are formed through a small, but important, pathway (α) present in the reaction of isoprene and OH (+O_2) in the presence of NO. The dominant pathway ($1-\alpha$) forms NO_2 and promotes ozone production. The formation of the two IHN isomers shown here (1,2-IHN and 4,3-IHN; dashed boxes) represent more than 90% of the IHN produced at atmospherically relevant RO_2 lifetimes (17). We note that the α to 1,2-IHN ($14 \pm 3\%$) is very similar to the α to 4,3-IHN ($13 \pm 3\%$) (18). Once formed, 1,2-IHN and 4,3-IHN can undergo deposition, oxidation, or incorporation into aerosol, where they can hydrolyze. The branching between IHN-loss pathways directly affects isoprene's impact on NO_x and oxidant levels. IHN-loss pathways that result in NO_x recycling are highlighted in blue, while those that result in the permanent loss of NO_x are red.

pathway could contribute significantly to HNO_3 formed over continental regions (28, 31–35). Photolysis has also been proposed (25). Unlike hydrolysis, photolysis of organic nitrates is expected to release NO_2 back into the atmosphere, contributing to tropospheric ozone production downwind of sources (22, 35).

Here, we used newly developed instrumentation (36) to monitor changes in the isomer distribution of IHN during a 2017 summer field study conducted in Pasadena, CA. These ambient observations are interpreted using a combination of laboratory chamber experiments, aqueous hydrolysis experiments, and observationally constrained model simulations. We focus our analysis on the two most abundant isomers, 1,2-IHN and 4,3-IHN. Since 1,2-IHN and 4,3-IHN are thought to undergo similar atmospheric fates (Scheme 1), we use the ratio of their concentrations (1,2-IHN to 4,3-IHN; hereafter, referred to as "IHN isomer ratio," for simplicity) as a proxy for differences in their nonphotochemical loss.

This dataset suggests the 1,2-IHN isomer is rapidly lost via hydrolysis in the atmosphere at a rate competitive with other oxidation and deposition pathways. In addition, global simulations suggest that this loss pathway greatly impacts the global concentration of NO_x, ozone, and nitric acid.

Results and Discussion

Field Observations. Hourly measurements of the ambient concentrations of the IHN isomers were obtained between August 1 and 17, 2017 (37) using a gas chromatography–chemical ionization mass spectrometer (GC-CIMS) deployed atop the main Caltech library (44 m above ground level), which is located on the California Institute of Technology (Caltech) campus in Pasadena, CA: $[OH]_{avg,\ peak} = 5 \times 10^6$ molecules cm^{-3} (38); $[NO]_{avg,\ daytime} =$ 2.5 parts per billion by volume (ppbv). Details of the field site, measurement technique and data processing are provided in *Materials and Methods* and *SI Appendix*.

Daytime observations (1000 to 2000 hours local time) of 1,2-IHN and 4,3-IHN from Caltech (Fig. 1) suggest an additional IHN sink is present in the atmosphere that disproportionately affects the 1,2-IHN isomer. We observed a daily, rapid decline of the IHN isomer ratio starting in the midafternoon (around 1500 hours local time). Chromatograms collected at this site (Fig. 2) (39) illustrate that this was caused by a drop in the concentration of 1,2-IHN relative to 4,3-IHN. However, these observations are not explained using known gas-phase chemistry as the gas-phase lifetime of 1,2-IHN is expected to be longer than 4,3-IHN due to its slower reaction rate with OH (21). This is

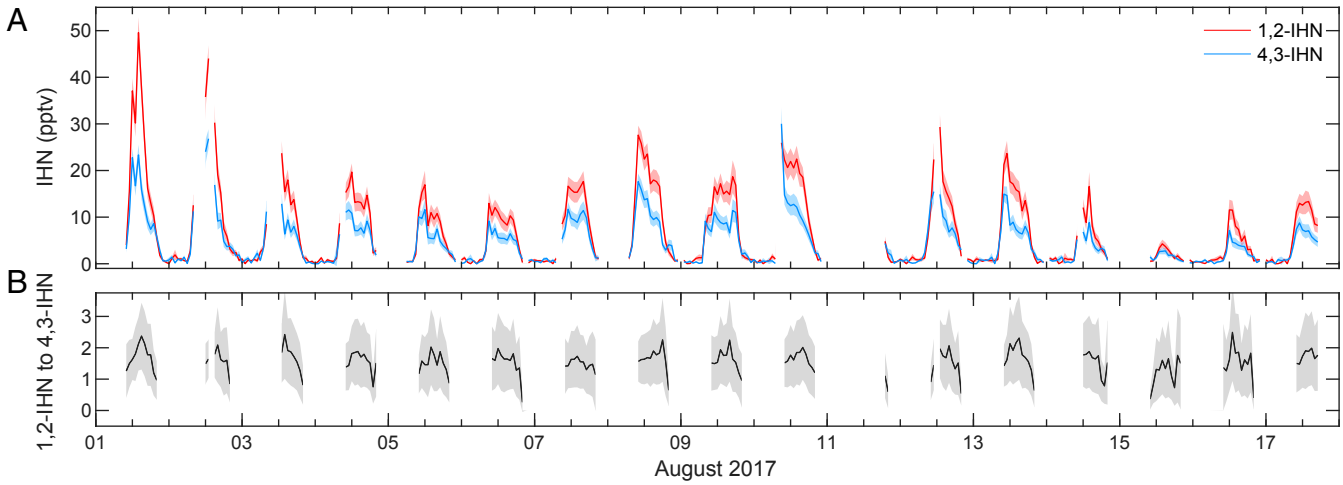

Fig. 1. (*A*) Time series of 1,2-IHN (red) and 4,3-IHN (blue) as measured by the GC-CIMS during the Caltech field study. Solid lines represent the hourly GC measurements, and the shaded regions encompass the error of those measurements. (*B*) The observed daytime (1000 to 2000 hours local time) isomer ratio of 1,2-IHN to 4,3-IHN during the Caltech field study.

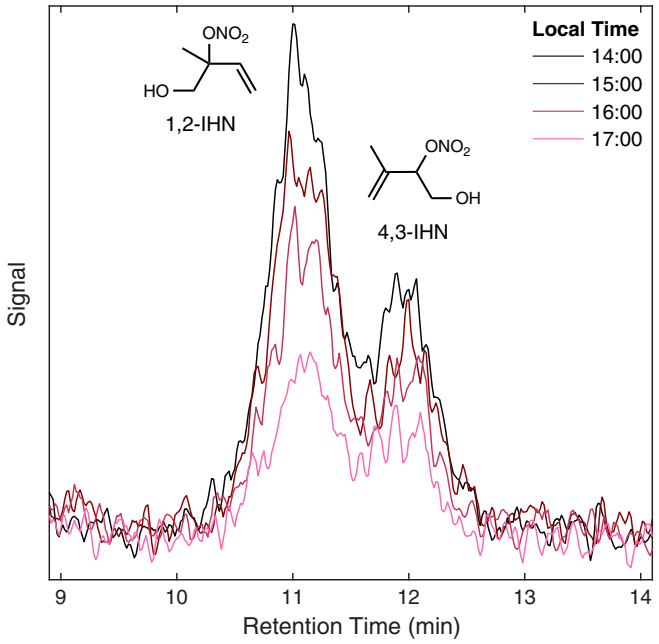

Fig. 2. Four chromatograms of IHN collected during the Caltech field study on August 1, 2017 show that the peak area of 1,2-IHN declines more rapidly than 4,3-IHN in the late afternoon.

verified in Fig. 3, where the IHN isomer ratio simulated with a one-dimensional (1-D) atmospheric model (red) consistently overpredicts the observed ratio (black), with the largest discrepancies occurring in the evening. The model shows that when considering only the gas-phase isoprene chemistry (18) and dry deposition (20), the IHN isomer ratio should steadily increase during this time in contrast with observations.

Laboratory Evidence for IHN Hydrolysis

Chamber Studies. Isoprene-oxidation experiments performed in a 24-m^3 chamber (*SI Appendix*, section 3) suggest that 1,2-IHN is hydrolyzed much faster than 4,3-IHN, lending one possible explanation to the observed trend of the ambient IHN isomer ratio measured at Caltech. In the dark chamber, the lifetime of the 1,2-IHN isomer decreased from 45 min at 50% relative humidity (RH) to 15 min at 85% RH—whereas no change in the 4,3-IHN lifetime was observed. In addition, chromatograms obtained from these experiments (*SI Appendix*, Fig. S2) mirrored those collected in the field (Fig. 2). Accompanying signals of IHN hydrolysis products, such as the isoprene diol and a small yield of 1,4-IHN (17), were observed.

During these experiments, it is likely that IHN hydrolysis was occurring within a condensed-phase reservoir formed by the uptake of water at high RH by salts that had been previously deposited on the chamber walls. Similar experiments with high levels of added ammonium sulphate seed (up to 500 μg m^{-3}) did not measurably alter the decay rate. In contrast, gas-phase experiments performed in a clean 1-m^3 Teflon chamber bag did not show any decay of 1,2-IHN at high RH (>80%) over a 12-h period. Unfortunately, this complicates interpretation of the loss rates observed in the 24-m^3 chamber, as they are likely dependent on the volume of liquid material on the walls, as well as the mixing and transport processes.

^{1}H NMR. As we were unable to provide a quantitative constraint on the hydrolysis loss through the chamber experiments, we use a newly developed synthetic route to 1,2-IHN (*SI Appendix*, section 3) with ^{1}H NMR to probe the kinetics of the 1,2-IHN hydrolysis loss (31). For this experiment, a known volume of synthesized 1,2-IHN was added to a known volume of deuterated chloroform ($CDCl_3$), rapidly mixed, and quickly analyzed using ^{1}H NMR (*SI Appendix*, Fig. S3). In a similar fashion, 1,2-IHN was added to deuterium oxide (D_2O), mixed, and analyzed. No 1,2-IHN ^{1}H NMR signals remained in the D_2O sample (elapsed time from mixing to completion of analysis, <1 min). Based on the signal-to-noise ratio of the 1,2-IHN ^{1}H NMR signals in the CD_3Cl sample, we assign an upper limit of 10 s for the aqueous hydrolysis lifetime of 1,2-IHN in D_2O at 298 K (*SI Appendix*, section 3). For comparison, Jacobs et al. (40) measured the 4,3-IHN hydrolysis lifetime to be approximately 17.5 h in D_2O. The large difference in the hydrolysis lifetimes of these two isomers is consistent with both our chamber and field observations.

Model Simulations of IHN Hydrolysis. Based on laboratory evidence, we incorporated condensed-phase hydrolysis into a 1-D box model to test whether this loss is consistent with the observed diurnal profile of the IHN isomer ratio observed at Caltech. Details of this model are provided in *Materials and Methods* and *SI Appendix*. Briefly, the model uses the recently developed condensed isoprene mechanism (18) and K-theory (41) to simulate the formation, oxidation, and mixing of IHN isomers in an atmospheric column representative of conditions observed at the Calfiornia Nexus Los Angeles Ground Site (CalNex-LA)

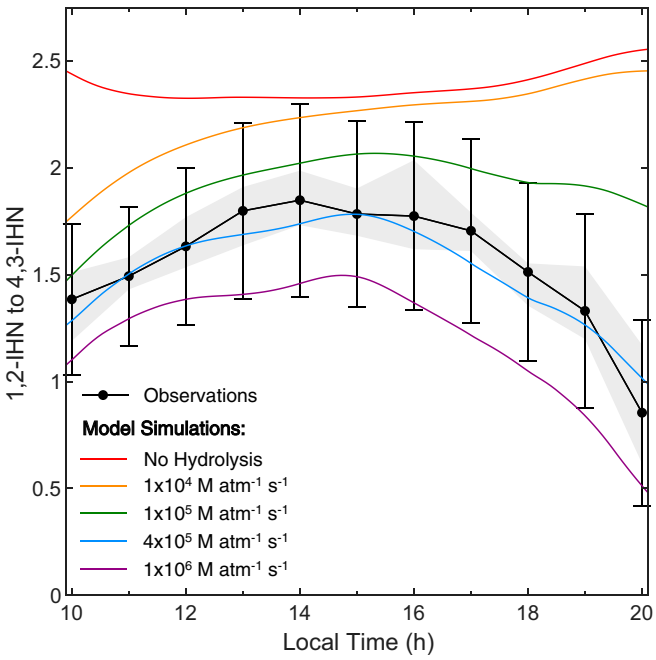

Fig. 3. Comparison of observed (black) and modeled (colored lines) diurnal profiles of the IHN isomer ratio from the Caltech field study. Each black dot represents the median of the hourly IHN isomer ratios, while the gray region encompasses the 25th and 75th percentile values, and the error bars represent the error in the study-averaged results. The model simulation that includes dry deposition and gas-phase chemistry only (red) overpredicted the IHN ratio, particularly in the afternoon, when 4,3-IHN loss should be faster than that of 1,2-IHN due to OH oxidation. Inclusion of a temperature-dependent (*SI Appendix*, Fig. S6) condensed-phase hydrolysis loss coefficient of 1,2-IHN (defined as, k^*_{hydro}, a product of Henry's law constant and aqueous hydrolysis rate [$K_H \times k_{(aq)}$]) enables the model to reproduce the observed IHN isomer ratio using $k^*_{hydro} = 4 \times 10^5$ M atm^{-1} s^{-1} (blue).

(42), which took place on the Caltech campus in 2010. Aerosol liquid water (ALW) concentrations used in the model were calculated with ISORROPIA-II (43), using aerosol measurements obtained from CalNex-LA. Our calculated ALW compares well with results presented in Guo et al. (44). We assume that IHN uptake into the particle is reversible and in instantaneous equilibrium with gas-phase concentrations (45).

The Henry's law coefficient (K_H) of the 1,2-IHN is not known, and, from our NMR study, we have only a lower limit to $k_{(aq)}$. However, provided that $k_{(aq)}$ is less than a few 100 s^{-1}, the hydrolysis loss rate of 1,2-IHN on aerosol (referred to here as the hydrolysis loss coefficient (49), k^*_{hydro}) will occur as the product of these two terms. Therefore, we can vary k^*_{hydro} in our simulations to find the best match to the observed diurnal profile of the IHN isomer ratio.

Fig. 3 shows how modeled IHN isomer ratios compare to observations over a range of hydrolysis loss coefficients (46), with the best agreement occurring when $k^*_{hydro} = 4 \times 10^5$ M atm^{-1} s^{-1} (blue). At this rate, the heterogenous lifetime of 1,2-IHN against hydrolysis ranges between 4 and 7 h in the daytime driven by changes in ALW (3.6 to 6 μg m^{-3}). This loss contributes to ~30% of the mid-day loss of the 1,2-IHN isomer, with that fraction increasing to over 50% in the evening (after 1800 hours local time), as a result of both the increased ALW concentrations and lower OH.

We note that ALW is highly sensitive to both humidity and aerosol composition, and so k^*_{hydro} will be quite variable depending on local conditions. For example, during the Southern Oxidant and Aerosol Study campaign, which took place in the southeastern United States, ALW was typically 1 to 5 μg m^{-3} on most afternoons, and median mass concentrations exceeded 15 μg m^{-3} in the morning (0600 to 0900 hours local time) (47). Furthermore, although not important at the Pasadena field site, hydrolysis by boundary layer cloud processing will also be efficient in many places. To the extent that this is important, our simulations described below will underrepresent the importance of IHN hydrolysis globally.

Our model results are relatively insensitive to additional parameters such as the assumed IHN-deposition velocity, horizontal advective loss, or vertical mixing rates (*SI Appendix*, section 5). However, we find that the modeled ratio is quite sensitive to our assumed ALW. The ALW in our model was estimated from aerosol measurements collected in May to July, which, on average, is a more humid time period than August. In addition, the United States has experienced a steady decline in SO_2 emissions since 2010 (48), which has been repeatedly linked to the reduction of sulphate in aerosols in the summer (49, 50). As sulfate affects the hygroscopicity of the particle, lower humidity and sulfate concentrations would result in lower ALW (51) than would be predicted using CalNex-LA ALW measurements. If we have overestimated ALW, then the inferred k^*_{hydro} is too small.

Atmospheric Implications. We have implemented the inferred k^*_{hydro} of 1,2-IHN into the global chemical transport model, GEOS-Chem, that has been recently updated to reflect the most recent laboratory studies of isoprene photochemistry (52, 53). Shown in Fig. 4 is the change in simulated NO and O_3 when we add 1,2-IHN hydrolysis with a rate similar to that of our 1-D model (in this case, $k^*_{hydro} = 3 \times 10^5$ M atm^{-1} s^{-1}; *SI Appendix*, section 6) to the standard GEOS-Chem model. Consistent with the findings of Paulot et al. (11), we find that over forested regions, the loss of NO_x via the formation of IHN and its subsequent conversion to HNO_3 through condensed-phase hydrolysis (*SI Appendix*, Fig. S8) leads to large reductions in simulated NO levels in the tropics (independent of seasonality; Fig. 4*A*) and during the Northern Hemisphere summer (Fig. 4*B*). This change, in turn, substantially reduces the calculated concentrations of OH (*SI Appendix*, Fig. S9) and O_3 (Fig. 4 *C* and *D*). Of note, surface ozone in the southeastern United States is ~5 parts per billion (ppb) lower in the summer with the addition of 1,2-IHN hydrolysis (Fig. 4*D*)—a change that brings the simulations into agreement with ground-based observations. Previously, to properly simulate surface ozone in GEOS-Chem, an ad hoc reduction between 30 and 60% in NO_x emissions had been suggested (54).

Although our laboratory measurements are unable to quantify the aqueous hydrolysis rate of 1,2-IHN, we find that the global impact of this chemistry is largely insensitive to the assumed hydrolysis loss coefficient, provided that k^*_{hydro} is at least 3×10^5 M atm^{-1} s^{-1} (*SI Appendix*, Fig. S7). The insensitivity of our simulations to k^*_{hydro} above most of the world's forests is a result of the low calculated OH levels ($[OH]_{avg} < 5 \times 10^5$ molecules cm^{-3}; *SI Appendix*, Fig. S10), different from the conditions of the Caltech field site. With such low OH, the gas-phase lifetime of IHN approaches 24 h, and, as a result, hydrolysis outcompetes all other IHN loss processes.

In conclusion, we present a rare observational constraint on the isomer-specific fate of IHN using both laboratory and field measurements obtained using GC-CIMS. Our data suggest that global atmospheric photochemistry is remarkably sensitive to the hydrolysis of a single isoprene hydroxy nitrate isomer, 1,2-IHN. Using GEOS-Chem, we simulate the effect a hydrolysis rate of at least 3×10^5 M atm^{-1} s^{-1} has on NO, O_3, OH, and HNO_3 concentrations in the lower atmosphere. We find that this added loss process represents the majority of the IHN loss over forested regions, resulting in a substantial decrease of simulated NO in the tropics (year-round) and in the Northern Hemisphere during the summer. This drop in NO, in turn, results in lower concentrations of simulated ozone—allowing for better agreement between this model and ground-based observations, especially in the southeastern United States. Lastly, 1,2-IHN hydrolysis acts as a significant source of HNO_3 that is on par with OH + NO_2.

Materials and Methods

Description of Field Site. Measurements described here were collected from a field site located at the Caltech campus in Pasadena, CA, which is located in the Los Angeles metropolitan area approximately 18 km northeast of downtown Los Angeles (DTLA) and 7 km south of the San Gabriel Mountains. The instrument was located on the southwest corner of the roof of the 44-m tall Caltech library (lat 34.137; long −118.126) from August 1 to 17, 2017, sampling into the daytime prevailing winds, which arrived predominantly from the south. Because of its proximity to DTLA, the site experienced high levels of anthropogenic pollution ($[NO]_{avg,\ daytime}$ = 2.5 ppbv). In addition, local vegetation is made up of known isoprene emitters (55), allowing for local biogenic emissions to influence the site.

In addition, a weather station was colocated with our main GC-CIMS instrument to monitor relative humidity (%), air temperature (°C), barometric pressure (mbar), solar radiation (W/m^2), wind speed (m/s), and wind direction. Additional details regarding this field site are provided in *SI Appendix*.

Isomer Measurements. The GC-CIMS instrumentation, and details of its field operation, has been described previously in the literature (36). Briefly, ambient air was pulled at a high flow rate (~2,000 standard liters per minute) through a Teflon-coated glass inlet (3.8-cm inner diameter; 76.2 cm long). A subsampled portion of this gas stream was then directed into the CIMS, either directly or after analytes are separated on a 1-m GC column. Analyte concentrations were quantified using a CF_3O^- reagent ion, which is sensitive toward the detection of oxygenated multifunctional compounds such as organic peroxides and nitrates (16, 56–58). In the field, the instrument collected data in automated 1-h cycles, with GC separation occurring in the latter half hour.

Laboratory experiments were performed on a prototype version of the GC-CIMS field instrument. Analytes were trapped on a portion of a 1-m column that was submerged in an isopropanol bath chilled to approximately

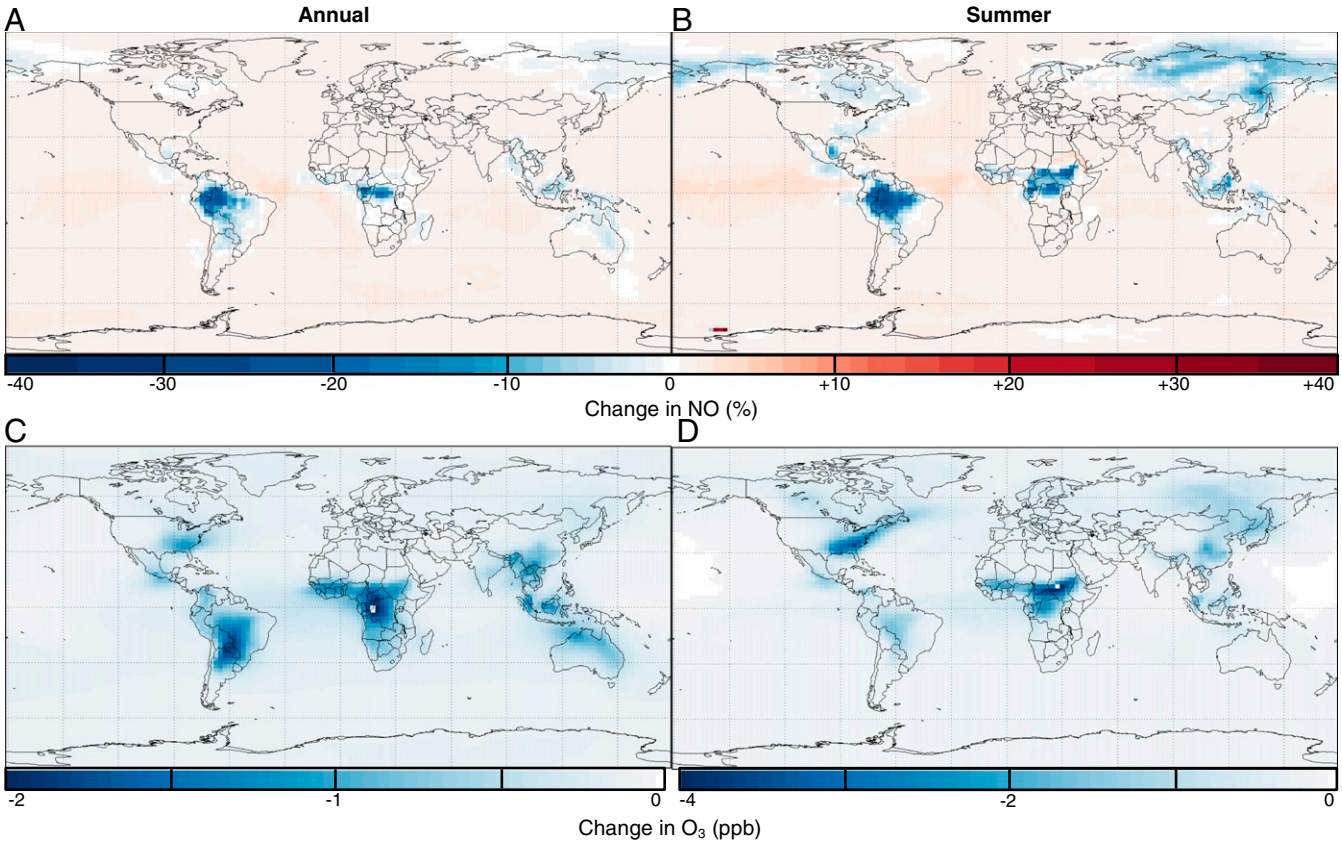

Fig. 4. The standard GEOS-Chem model was updated to include an 1,2-IHN hydrolysis rate of $k^*_{hydro} = 3 \times 10^5$ M atm^{-1} s^{-1}. The impact of this loss on NO and ozone was then assessed through both annual and summer (July 1 to 31) simulations conducted in the lowest 1 km of the atmosphere. The addition of this IHN sink resulted in a ~40% decrease in NO in the tropics throughout the year (*A*) and a lesser, but still substantial, decrease in the Northern Hemisphere during the summer (*B*), with respect to the base model. Likewise, O_3 concentrations also experienced the same spatial and seasonal decrease as NO (*C* and *D*). Of note, surface ozone in the southeastern United States is 5 ppb lower in the summer (*D*), causing this updated model to better agree with ground-based observations.

−20° C. The column was then heated within a Varian CP-3800 GC oven. The column effluent was then directed into a CF_3O^- CIMS.

Measurement uncertainty from field data arose from low analyte signal, caused by a combination of low ambient concentrations and the high instrument dilution needed to prevent simultaneous trapping of water (36). Additional details regarding data processing and measurement uncertainties can be found in *SI Appendix*.

1-D Atmospheric Model. A 1-D atmospheric model was used to interpret ambient measurements collected during the Caltech field study. The model simulates the emission, deposition, vertical transport, and photochemical oxidation of 250 species in an atmospheric column tuned to replicate conditions observed during the 2010 CalNex-LA campaign, which also took place on the Caltech campus. The model combines the latest version of the Regional Atmospheric Chemistry Mechanism (59) with the condensed isoprene-oxidation mechanisms described by Wennberg et al. (18) and IHN deposition rates based on measurements made by Nguyen et al. (20). Vertical transport is simulated in the model using K-theory (41), and its implementation in the model is described in more detail in *SI Appendix*.

Given the uncertainty in local isoprene emissions due to vegetation heterogeneity in and around the Pasadena area, sensitivity tests were performed to determine a reasonable emission rate that produced agreement between measured and modeled isoprene concentrations. ALW concentrations used to model IHN partitioning were calculated using ISORROPIA-II (43) using inputs of temperature, RH, and inorganic aerosol components measured during CalNex-LA. The calculated ALW agreed well with that reported by Guo et al. (44).

Data Availability. Atmospheric trace gas measurements and model output data have been deposited in the California Institute of Technology Research Data Repository CaltechDATA. IHN isomer concentration data used here are available online (http://doi.org/10.22002/D1.971) along with the chromatograms collected at the field site (http://doi.org/10.22002/D1.1671), the output results of the 1-D atmospheric model (http://doi.org/10.22002/D1.1672), and the updated isoprene mechanism used in the global chemical transport model (http://doi.org/10.22002/D1.247). GEOS-Chem is available for public use at http://geos-chem.org/.

ACKNOWLEDGMENTS. Development of the GC-CIMS was supported by the NSF Major Research Instrumentation Program under Grant AGS-1428482 and the field and laboratory studies it participated in were supported by additional NSF funding (Grant AGS-1240604). We thank the Caltech campus and affiliated staff for accommodating our 2017 field study. Work performed by K.T.V. and H.M.A. was also supported by NSF through the Graduate Research Fellowship.

1. E. C. Browne, R. C. Cohen, Effects of biogenic nitrate chemistry on the NOx lifetime in remote continental regions. *Atmos. Chem. Phys.* **12**, 11917–11932 (2012).
2. H. Simon, A. Reff, B. Wells, J. Xing, N. Frank, Ozone trends across the United States over a period of decreasing NO_x and VOC emissions. *Environ. Sci. Technol.* **49**, 186–195 (2015).
3. A. E. Perring, S. E. Pusede, R. C. Cohen, An observational perspective on the atmospheric impacts of alkyl and multifunctional nitrates on ozone and secondary organic aerosol. *Chem. Rev.* **113**, 5848–5870 (2013).
4. J. Mao *et al.*, Southeast atmosphere studies: Learning from model-observation syntheses. *Atmos. Chem. Phys.* **18**, 2615–2651 (2018).
5. L. Xu, S. Suresh, H. Guo, R. J. Weber, N. L. Ng, Aerosol characterization over the southeastern United States using high-resolution aerosol mass spectrometry: Spatial and seasonal variation of aerosol composition and sources with a focus on organic nitrates. *Atmos. Chem. Phys.* **15**, 7307–7336 (2015).
6. A. W. Rollins *et al.*, Evidence for NOx control over nighttime SOA formation. *Science* **337**, 1210–1212 (2012).

7. M. Trainer *et al.*, Observations and modeling of the reactive nitrogen photochemistry at a rural site. *J. Geophys. Res. Atmos.* **96**, 3045–3063 (1991).
8. S. Wu *et al.*, Why are there large differences between models in global budgets of tropospheric ozone? *J. Geophys. Res.* **112**, D05302 (2007).
9. L. W. Horowitz *et al.*, Observational constraints on the chemistry of isoprene nitrates over the eastern United States. *J. Geophys. Res. Atmos.* **112**, D12S08 (2007).
10. M. R. Beaver *et al.*, Importance of biogenic precursors to the budget of organic nitrates: Observations of multifunctional organic nitrates by CIMS and TD-LIF during BEARPEX 2009. *Atmos. Chem. Phys.* **12**, 5773–5785 (2012).
11. F. Paulot, D. K. Henze, P. O. Wennberg, Impact of the isoprene photochemical cascade on tropical ozone. *Atmos. Chem. Phys.* **12**, 1307–1325 (2012).
12. J. Mao *et al.*, Ozone and organic nitrates over the eastern United States: Sensitivity to isoprene chemistry. *J. Geophys. Res. Atmos.* **118**, 11256–11268 (2013).
13. O. J. Squire *et al.*, Influence of isoprene chemical mechanism on modeled changes in tropospheric ozone due to climate and land use over the 21st century. *Atmos. Chem. Phys.* **15**, 5123–5143 (2015).
14. A. G. Carlton *et al.*, Synthesis of the southeast atmosphere studies: Investigating fundamental atmospheric chemistry questions. *Bull. Am. Meteorol. Soc.* **99**, 547–567 (2018).
15. J. Li *et al.*, Decadal changes in summertime reactive oxidized nitrogen and surface ozone over the southeast United States. *Atmos. Chem. Phys.* **18**, 2341–2361 (2018).
16. F. Paulot *et al.*, Isoprene photooxidation: New insights into the production of acids and organic nitrates. *Atmos. Chem. Phys.* **9**, 1479–1501 (2009).
17. A. P. Teng, J. D. Crounse, P. O. Wennberg, Isoprene peroxy radical dynamics. *J. Am. Chem. Soc.* **139**, 5367–5377 (2017).
18. P. O. Wennberg *et al.*, Gas-phase reactions of isoprene and its major oxidation products. *Chem. Rev.* **118**, 3337–3390 (2018).
19. J. A. Fisher *et al.*, Organic nitrate chemistry and its implications for nitrogen budgets in an isoprene- and monoterpene-rich atmosphere: Constraints from aircraft ($SEAC^4RS$) and ground-based (SOAS) observations in the southeast US. *Atmos. Chem. Phys.* **16**, 5969–5991 (2016).
20. T. B. Nguyen *et al.*, Rapid deposition of oxidized biogenic compounds to a temperate forest. *Proc. Natl. Acad. Sci. U.S.A.* **112**, E392–E401 (2015).
21. L. Lee, A. P. Teng, P. O. Wennberg, J. D. Crounse, R. C. Cohen, On rates and mechanisms of OH and O_3 reactions with isoprene-derived hydroxy nitrates. *J. Phys. Chem. A* **118**, 1622–1637 (2014).
22. J. F. Müller, J. Peeters, T. Stavrakou, Fast photolysis of carbonyl nitrates from isoprene. *Atmos. Chem. Phys.* **14**, 2497–2508 (2014).
23. P. Giacopelli, K. Ford, C. Espada, P. B. Shepson, Comparison of the measured and simulated isoprene nitrate distributions above a forest canopy. *J. Geophys. Res. Atmos.* **110**, D01304 (2005).
24. S. Liu *et al.*, Hydrolysis of organonitrate functional groups in aerosol particles. *Aerosol Sci. Technol.* **46**, 1359–1369 (2012).
25. F. Xiong *et al.*, Observation of isoprene hydroxynitrates in the southeastern United States and implications for the fate of NOx. *Atmos. Chem. Phys.* **15**, 11257–11272 (2015).
26. G. M. Wolfe *et al.*, Quantifying sources and sinks of reactive gases in the lower atmosphere using airborne flux observations. *Geophys. Res. Lett.* **42**, 8231–8240 (2015).
27. C. M. Boyd *et al.*, Secondary organic aerosol formation from the β-pinene+NO_3 system: Effect of humidity and peroxy radical fate. *Atmos. Chem. Phys.* **15**, 7497–7522 (2015).
28. J. D. Rindelaub, K. M. McAvey, P. B. Shepson, The photochemical production of organic nitrates from α-pinene and loss via acid-dependent particle phase hydrolysis. *Atmos. Environ.* **100**, 193–201 (2015).
29. J. K. Bean, L. H. Ruiz, Gas-particle partitioning and hydrolysis of organic nitrates formed from the oxidation of α-pinene in environmental chamber experiments. *Atmos. Chem. Phys.* **16**, 2175–2184 (2016).
30. D. A. Day, S. Liu, L. M. Russell, P. J. Ziemann, Organonitrate group concentrations in submicron particles with high nitrate and organic fractions in coastal southern California. *Atmos. Environ.* **44**, 1970–1979 (2010).
31. A. I. Darer, N. C. Cole-Filipiak, A. E. O'Connor, M. J. Elrod, Formation and stability of atmospherically relevant isoprene-derived organosulfates and organonitrates. *Environ. Sci. Technol.* **45**, 1895–1902 (2011).
32. K. S. Hu, A. I. Darer, M. J. Elrod, Thermodynamics and kinetics of the hydrolysis of atmospherically relevant organonitrates and organosulfates. *Atmos. Chem. Phys.* **11**, 8307–8320 (2011).
33. E. C. Browne *et al.*, Observations of total $RONO_2$ over the boreal forest: NOx sinks and HNO_3 sources. *Atmos. Chem. Phys.* **13**, 4543–4562 (2013).
34. P. S. Romer *et al.*, The lifetime of nitrogen oxides in an isoprene-dominated forest. *Atmos. Chem. Phys.* **16**, 7623–7637 (2016).
35. A. Zare *et al.*, A comprehensive organic nitrate chemistry: Insights into the lifetime of atmospheric organic nitrates. *Atmos. Chem. Phys.* **18**, 15419–15436 (2018).
36. K. T. Vasquez *et al.*, Low-pressure gas chromatography with chemical ionization mass spectrometry for quantification of multifunctional organic compounds in the atmosphere. *Atmos. Meas. Tech.* **11**, 6815–6832 (2018).
37. K. T. Vasquez, L. Xu, J. D. Crounse, P. O. Wennberg, IHN GC data from 2017 Caltech Roof Study (Version 1.0). CaltechDATA. http://doi.org/10.22002/D1.971. Deposited 4 July 2018.
38. S. M. Griffith *et al.*, Measurements of hydroxyl and hydroperoxy radicals during CalNex-LA: Model comparisons and radical budgets. *J. Geophys. Res. Atmos.* **121**, 4211–4232 (2016).
39. K. T. Vasquez, L. Xu, J. D. Crounse, P. O. Wennberg, GC chromatograms from 2017 Caltech Roof Study (Version 1.0). CaltechDATA. http://doi.org/10.22002/D1.1671. Deposited 17 November 2020.
40. M. I. Jacobs, W. J. Burke, M. J. Elrod, Kinetics of the reactions of isoprene-derived hydroxynitrates: Gas phase epoxide formation and solution phase hydrolysis. *Atmos. Chem. Phys.* **14**, 8933–8946 (2014).
41. G. M. Wolfe, J. A. Thornton, The Chemistry of Atmosphere-Forest Exchange (CAFE) model - Part 1: Model description and characterization. *Atmos. Chem. Phys.* **11**, 77–101 (2011).
42. T. B. Ryerson *et al.*, The 2010 California research at the nexus of air quality and climate change (CalNex) field study. *J. Geophys. Res. Atmos.* **118**, 5830–5866 (2013).
43. C. Fountoukis, A. Nenes, ISORROPIA II: A computationally efficient thermodynamic equilibrium model for K^+-Ca^{2+}-Mg^{2+}-NH_4^+-Na^+-SO_4^{2-}-NO_3^--Cl^--H_2O aerosols. *Atmos. Chem. Phys.* **7**, 4639–4659 (2007).
44. H. Guo *et al.*, Fine particle pH and gas–particle phase partitioning of inorganic species in Pasadena, California, during the 2010 CalNex campaign. *Atmos. Chem. Phys.* **17**, 5703–5719 (2017).
45. H. O. T. Pye, A. W. H. Chan, M. P. Barkley, J. H. Seinfeld, Global modeling of organic aerosol: The importance of reactive nitrogen (NO_x and NO_3). *Atmos. Chem. Phys.* **10**, 11261–11276 (2010).
46. B. C. Schulze, K. T. Vasquez, J. D. Crounse, P. O. Wennberg, IHN hydrolysis 1D model results. CaltechDATA. http://doi.org/10.22002/D1.1672. Deposited 17 November 2020.
47. T. K. V. Nguyen *et al.*, Trends in particle-phase liquid water during the southern oxidant and aerosol study. *Atmos. Chem. Phys.* **14**, 10911–10930 (2014).
48. US Environmental Protection Agency, Sulfur dioxide trends (2018). https://www.epa.gov/air-trends/sulfur-dioxide-trends. Accessed 13 April 2019.
49. J. L. Hand, B. A. Schichtel, W. C. Malm, M. L. Pitchford, Particulate sulphate ion concentration and so_2 emission trends in the United States from the early 1990s through 2010. *Atmos. Chem. Phys.* **12**, 10353–10365 (2012).
50. F. Paulot, S. Fan, L. W. Horowitz, Contrasting seasonal responses of sulfate aerosols to declining SO_2 emissions in the Eastern U.S.: Implications for the efficacy of SO_2 emission controls. *Geophys. Res. Lett.* **44**, 455–464 (2017).
51. A. G. Carlton, B. J. Turpin, Particle partitioning potential of organic compounds is highest in the Eastern US and driven by anthropogenic water. *Atmos. Chem. Phys.* **13**, 10203–10214 (2013).
52. K. H. Bates, D. J. Jacob, A new model mechanism for atmospheric oxidation of isoprene: Global effects on oxidants, nitrogen oxides, organic products, and secondary organic aerosol. *Atmos. Chem. Phys.* **19**, 9613–9640 (2019).
53. K. H. Bates, P. O. Wennberg, Isoprene oxidation model (Version 5). CaltechDATA. http://doi.org/10.22002/D1.247. Deposited 20 July 2017.
54. K. R. Travis *et al.*, Why do models overestimate surface ozone in the southeast United States? *Atmos. Chem. Phys.* **16**, 13561–13577 (2016).
55. A. Guenther, P. Zimmerman, M. Wildermuth, Natural volatile organic compound emission rate estimates for U.S. woodland landscapes. *Atmos. Environ.* **28**, 1197–1210 (1994).
56. J. D. Crounse, K. A. McKinney, A. J. Kwan, P. O. Wennberg, Measurement of gas-phase hydroperoxides by chemical ionization mass spectrometry. *Anal. Chem.* **78**, 6726–6732 (2006).
57. J. M. St. Clair, D. C. McCabe, J. D. Crounse, U. Steiner, P. O. Wennberg, Chemical ionization tandem mass spectrometer for the in situ measurement of methyl hydrogen peroxide. *Rev. Sci. Instrum.* **81**, 094102 (2010).
58. N. Hyttinen *et al.*, Computational comparison of different reagent ions in the chemical ionization of oxidized multifunctional compounds. *J. Phys. Chem. A* **122**, 269–279 (2018).
59. W. S. Goliff, W. R. Stockwell, C. V. Lawson, The regional atmospheric chemistry mechanism, version 2. *Atmos. Environ.* **68**, 174–185 (2013).